DOI: 10.1002/chem.200902113

Cluster-Based Self-Assembly Route toward MoO_3 Single-Walled Nanotubes

Shi Hu, Xi Ling, Tian Lan, and Xun Wang*[a]

Abstract: MoO_3 has a unique rigid double-layer structure, which makes it a real challenge to prepare nanotubular structures. The controlled synthesis of MoO_3 single-walled nanotubes (SWNTs) is achieved through a cluster-based self-assembly route on the dodecanethiol/water interface. Various factors are studied at length, including precursor type, reaction time, temperature, pH value, and their influence on the morphology of products. The concept of "self-assembly—from simple clusters to nanostructures" is proposed here based on preliminary results from the synthesis of MoO_3 SWNTs, which provides a new aspect for traditional synthetic chemistry of nanomaterials and polyoxometalates.

Keywords: molybdenum · nanotubes · self-assembly · synthetic methods

Introduction

Since the discovery of carbon nanotubes in 1991,[1] the preparation of nanoscale one-dimensional hollow structures has stimulated great fervor in academia due to their prominent performance in the fields of electronics,[2] biotechnology,[3] catalysis,[4] sensing,[5] field emitters,[6] separation,[7] energy storage,[8] and nanofluidics.[9] On the other hand, Tenne and co-workers reported the synthesis of a series of inorganic nanotubes based on layered transition-metal chalcogenides.[10] These species grew to include other layered compounds, including oxides,[11] halides,[12] metals,[13] and even materials with no layer structure through a template approach.[9] The nanotubular structure of these inorganic materials should combine the size effect with all kinds of intrinsic properties, for example, magnetic, catalytic, piezoelectric, and photoelectrical functions. However, compared with the attention and effort dedicated to carbon nanotubes, the field of inorganic nanotubes is less developed. Particularly, the controlled synthesis of single-walled inorganic nanotubes is far from successful,[14] since most of the reported inorganic nanotubes are based on template methods and their size is usually far above the critical length under which some unexpected properties arise. Hence, developing a new scheme for the production of single-walled noncarbon nanotubes is of great significance.

Three commonly known polymorphs of MoO_3 exist: the thermodynamically stable orthorhombic α phase, the metastable monoclinic β phase, and the hexagonal phase. The α phase, a wide-bandgap n-type semiconductor, has a unique layered structure in which distorted MoO_6 octahedra share four corners to form a plane and two planes join together by sharing octahedral edges along the [001] direction. All of these double layers stack up in the [010] direction (as shown in Figure 1a) with van der Waals forces acting between them. MoO_3 is of great importance to industrial catalysis, due to the variable oxidation state and a diversity of well-defined phases with different Mo/O ratios. The reversibility between oxidation states also endows it significant potential in the applications of electro-optical devices,[15] sensors,[16] information storage,[17] and rechargeable lithium batteries.[18]

Previously, reports of MoO_3-related nanostructures were limited to nanowires,[19] nanorods,[20] and nanobelts[18,21] that show little quantum confinement owing to their large size, yet Liu et al. have a separate report of a hollow MoO_3 nanosphere with a diameter of 5 nm through the use of block copolymer micelles.[22] Particularly, in these reports, nanostructure synthesis is taken from the phenomenological viewpoint of "trial and error", whereas chemists who synthesized Mo polyoxometalates used to think of the formation of the macromolecules as the self-assembly of small aqueous ions,[23] as such, a big gap lies between these two schools of scientists. Herein, we show that by tuning the pH of the system and the reaction intensity, different morphologies, including single-walled nanotubes (SWNTs), nanoparticles, and nanobelts, can be harvested in a controllable way, which results

[a] Dr. S. Hu, X. Ling, T. Lan, Prof. X. Wang
Department of Chemistry, Tsinghua University
Beijing, 100084 (P.R. China)
E-mail: wangxun@mail.tsinghua.edu.cn

Supporting information for this article is available on the WWW under http://dx.doi.org/10.1002/chem.200902113.

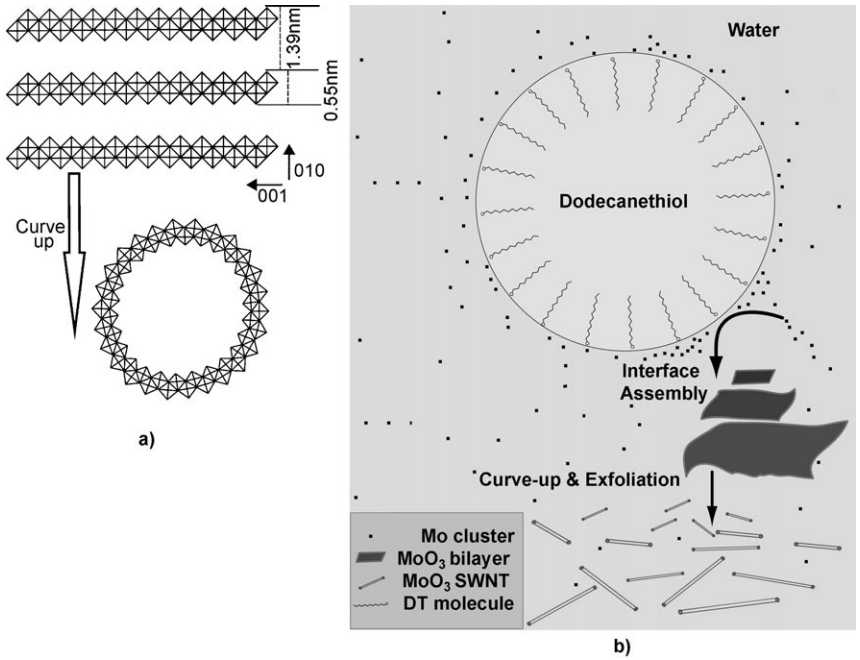

Figure 1. Schematic of SWNT formation at the oil–water interface.

from the assembly of simple clusters. Evidence for the formation of different nanostructures, especially SWNTs, is shown and various effects are carefully discussed. The concept of "self-assembly—from simple clusters to nanostructures" is clearly proposed here based on the preliminary results from the synthesis of MoO_3 SWNTs, which provides a new aspect of the traditional synthetic chemistry of nanomaterials and polyoxometalates. Furthermore, it should help to understand the chemical transformations in Mo chemistry and other fields of inorganic synthesis, especially in the nanostructure region.

Results and Discussion

Interface-mediated reactions have been well deployed for the synthesis and assembly of many different kinds of nanomaterials.[24] Heat reflux creates little droplets of one phase in another in which reactants in different phases meet at the interface to yield the product to a controlled degree. Successful examples of using a thiol/water interface leads to the preparation of monodisperse Ag_2S and Cu_2S nanocrystals.[25] As for MoO_3, the layered structure makes it possible to form nanotubes, whereas its double-layer feature makes it a real challenge to curve the layer into a tubular form. By resorting to the interface reaction of dodecanethiol (DT) with molybdic acid (MA) solution we successfully realized the preparation of MoO_3 SWNTs in hydrothermal autoclaves.[26] It is the oil/water interface that provides the driving force for the assembly of Mo clusters and enables the formation of MoO_3 SWNTs, as will be discussed below.

The choice of Mo precursor: It was found in previous work[26] that when MA solution reacts with DT under hydrothermal conditions, SWNTs are formed. As seen in the TEM pictures (Figure 2a), the copper grid is covered with a large area of films of interweaving nanotubes. These tubes are a few hundred nm long and uniform in diameter at around 6 nm. Formed together with the crossing NTs are some crystalline nanoparticles, the proportion of which increases with the oven temperature and reaction time. High-resolution transmission electron microscopy (HRTEM) pictures show more details about the NTs, revealing the thickness of the wall and the

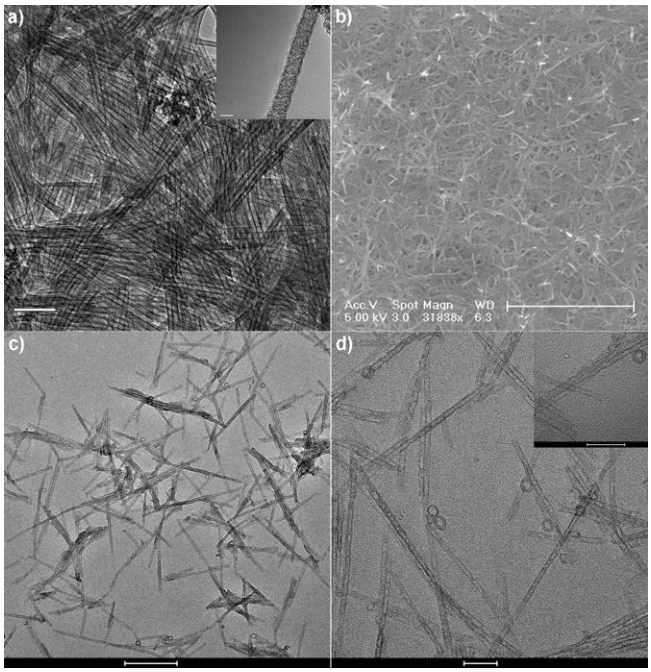

Figure 2. TEM images of the morphology of products after the reaction of dodecanethiol and MA (Beijing) as the precursor. Scales: a) 100 nm (main), 5 nm (inset); b) 1 μm; c) 200 nm; d) 50 nm (main and inset).

hollow chamber. Remarkably, long illumination times and high current density will destroy the tubular structure and prevents the acquisition of a clearer HRTEM image, as discussed in the following section. Representative large-area morphology of high-purity SWNT bundles is shown by SEM (Figure 2b). Furthermore, some double-walled fullerene-like spherical structures are observed at times on the carbon film

of the copper grid for samples without excess washing and centrifugation (Figure 2cand d), which is an interesting by-product for future investigation. This type of coexistence of NTs and fullerene is ubiquitous in layered nanomaterials.

However, when MA from different companies is used as the raw material, strikingly different results arise. A reaction carried out by using MA purchased from Beijing Reagent yielded MoO_3 SWNTs, MA from Sinopharm Chemical Reagent and Alfa Aesar leads to the production of MoO_2 nanoparticles, which could be attributed to the variations in composition and structure due to different manufacturing processes, as revealed by the XRD patterns (Figure S1 in the Supporting Information) and thermogravimetric analysis (TGA) curves of these products (Figure S2 in the Supporting Information).

To find a more stable and convincing alternative for the Mo source, ammonium molybdate (AM) was used in place of MA, but failed to generate SWNTs. Different degrees of acidification were tried by adding HCl to adjust the pH. It is shown that within a certain pH range, MoO_3 single-walled nanotubes could be obtained with almost the same morphology as those obtained from reactions involving MA (Figure 3a).

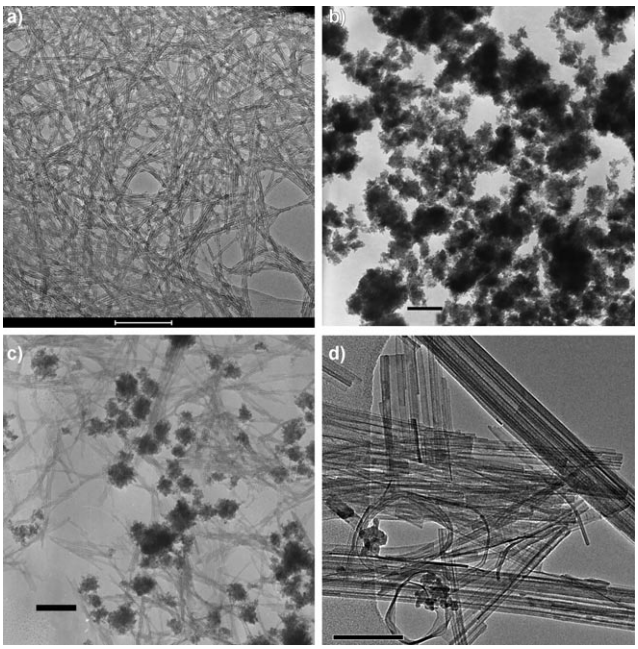

Figure 3. TEM images of products with variations in the choice of precursor: a) AM in place of MA (scale 200 nm); b) sodium molybdate in place of MA (scale 100 nm); c) OT in place of DT (scale 100 nm); d) MA (Beijing) pretreated at 250 °C for 2 h (scale 100 nm).

Furthermore, sodium molybdate (Na_2MoO_4) was tested as another alternative and the pH of the system was tuned by the addition of different amounts of HCl. Unfortunately, they inevitably led to the generation of MoO_2 or in quite an acidic environment, MoO_3 nanobelts were formed (Figure 3b). The presence of a large amount of NaCl after HCl addition should be responsible for this failure, as supported by a control experiment with the addition of NaCl to MA or acidified AM systems, which also destroyed the SWNTs.

The effect of thiol: The role played by the thiol in the synthesis is another key question. When octanethiol (OT) is used in place of DT the TEM images of the final products show the same morphology of SWNTs (Figure 3c). However, systematic experiments show that it is harder to suppress the amount of coexisting nanoparticles than by using DT. This is reasonable if we take into account the higher reactivity of OT compared with DT because of the shorter alkyl length, so it reduced the MoO_3 SWNTs to MoO_2 more easily. Nevertheless, it has extended the universality of the thiol/water reaction system.

It is a matter of course that different kinds of organic solvent should be tested in place of the thiol. However, many other water-immiscible organic solvents, such as dodecanol and alkanes, do not lead to the formation of SWNTs. Instead, they do not cause significant change to the aqueous solution of the Mo species. Moreover, the combination of these solvents with the thiol does destroy the reaction. For example, the addition of ethanol as a cosolvent leads to a decrease in SWNTs because the ethanol directly reduces the Mo^{VI} species and a large amount of MoO_2 appears in the product to the detriment of MoO_3 SWNTs. If cyclohexane, which is an inert substance to both the aqueous species and the DT, was added as a cosolvent then no precipitate was obtained, although the water phase turned a deep green, indicating the partial reduction of Mo^{VI}. This could also be understood as the destruction of the reaction interface between DT and water in the presence of cyclohexane; nonetheless, a detailed microscopic picture regarding the three-phase system is not in the scope of our discussion.

We also analyzed the composition of the upper oil phase in two samples at different extents of reaction by GC–MS and ^{1}H NMR spectroscopy (Figure 4). The GC result clearly shows the formation of a new species, the intensity of which increases with the extent of the reaction, and the mass spectrum gives a clear indication of the formation of didodecyl disulfide (DDS). Meanwhile, the ^{1}H NMR spectrum indicates the emergence of a new triplet at $\delta = 2.22$ ppm and a quintet at $\delta = 1.27$ ppm, the splitting of which exactly corresponds to the environment of hydrogen atoms on the α and β carbon atoms of DDS. Similar measurements have been conducted for the octanethiol system, which also indicates the presence of dioctyl disulfide. The possibility of air oxidation cannot be completely ruled out, but control experiments with no molybdenum source indicate that much less disulfide is present. Although disulfide acts as a capping ligand in the synthesis of colloidal gold, its presence in our system should contribute to the formation of SWNTs

Reaction intensity: Besides the precursor requirement, it is a very delicate reaction when the influence of temperature and reaction time is revealed. Temperature and time play a significant role in the successful control of MoO_3 SWNT for-

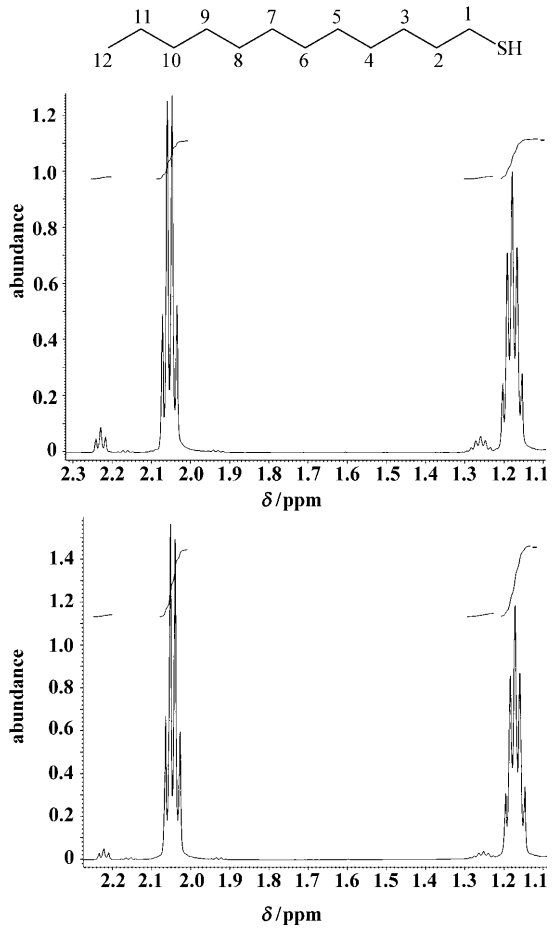

Figure 4. ^{1}H NMR of the oil phase after the reaction between dodecanethiol and Mo-containing solution with the upper spectrum obtained from a longer reaction time. The strength of the triplet at $\delta = 2.22$ ppm and the quintet at $\delta = 1.27$ ppm increases with increasing reaction time.

mation, since SWNTs are very sensitive to both factors. Inadequate temperature and time initiate no product formation, whereas overheating with either high temperatures or prolonged reaction time cause the partial or full destruction of MoO_3 SWNTs. Figure 5a shows the TEM images of the coexisting MoO_2 nanoparticles, with the lattice fringes in Figure 5b corresponding to the [110] interlayer distance of 0.34 nm. Suitable reaction times for different oven temperatures are listed in Table 1. As for the high sensitivity of this experiment, the time range may vary a little from oven to oven and should be readjusted accordingly.

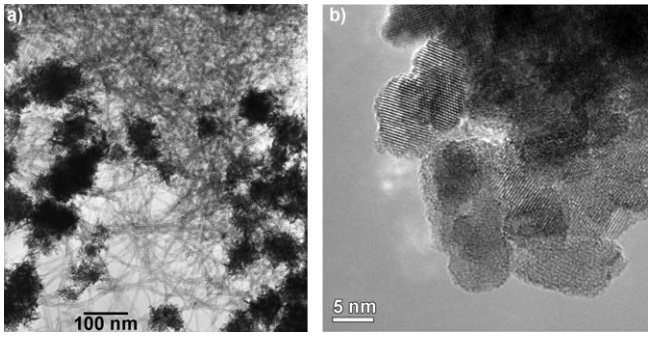

Figure 5. TEM images of products with increased reaction intensity.

Table 1. Reaction temperature and the corresponding reaction time for the synthesis of MoO_3 SWNTs

Oven temperature [°C]	Suitable reaction time [h]
190	32
195	20
200	12

pH-mediated cluster assembly: The choice of an appropriate molybdenum source and presence of thiol can be taken as a prerequisite for the successful synthesis of SWNTs. To find out the reasons for the influence of different raw materials on the morphology of the products, we adjusted the pH of the reaction in control experiments. By adding different amounts of HCl to the AM/H_2O/DT system, we found that nanobelts with parallel wrinkles form at low pH (Figure S3, inset, in the Supporting Information), whereas higher alkalinity finally causes the production of nanoparticles provided there is sufficient reaction time (Figure S4, inset, in the Supporting Information). The nanobelts can be indexed as hexagonal MoO_3 (Joint Committee on Powder Diffraction Standards (JCPDS) card number 21-0569), whereas the nanoparticles can be indexed as MoO_2 (JCPDS card number 32-0671), which are shown in Figures S3 and S4 in the Supporting Information. Furthermore, control experiments using heat-treated MA (Beijing) were conducted and no SWNTs were generated, but wrinkled nanobelts were formed, which is similar to what we found in the HCl overacidified system. The XRD spectra of these two samples in Figure S5 (in the Supporting Information) show that heating to 350 °C has transformed MA into MoO_3, whereas the experiment that was heated to 250 °C cannot be properly indexed. Thus, the success of MA (Beijing) over other brands of MA can be attributed to the presence of some impurities, such as H_2O and NH_3, which sets the pH of the system to an appropriate range, whereas heat treatment removes the NH_3 and raises the pH of the solution. The difference in the synthesis of SWNTs from different MA sources is, therefore, clearly an issue of pH.

The next question is why is pH so important? It has been extensively reported that MoO_3 with well-controlled nanobelt morphology can be produced in acidic media, although pH has a great influence on the form of Mo-containing species in the solution. The predominant species are $Mo_7O_{24}^{6-}$ and $H_xMo_7O_{24}^{(6-x)-}$ in neutral or near-neutral solution, whereas MoO_2^{2+} in acidic and MoO_4^{2-} in basic environments are the predominant species; thus pH has a great influence on the protonation state of Mo species, which can be found in the Raman spectra of a series of $[(NH_4)_6Mo_7O_{24}]$ solutions of different pH. The Raman spectra in Figure 6, obtained from samples with increasing amounts of HCl added, show that the center of peak 2 shifts from 945 to 960 cm^{-1}, indicating a gradual protonation pro-

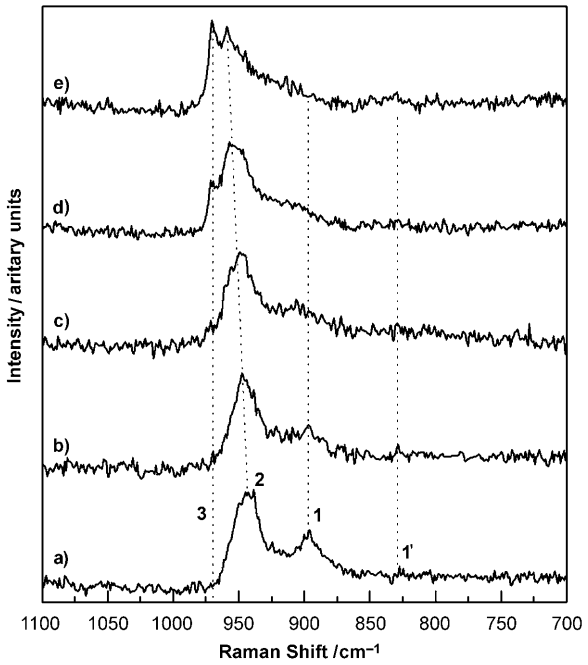

Figure 6. a)–e) Raman spectrum of a series of precursor solutions of AM with increasing levels of acidification.

cess from $Mo_7O_{24}^{6-}$ to $H_3Mo_7O_{24}^{3-}$, whereas the rising of peak 3 at 971 cm^{-1} indicates the emergence of an $Mo_8O_{26}^{4-}$ species. On the other hand, the characteristic peak of MoO_4^{2-} (**1** and **1′**) at around 897 and 837 cm^{-1} gradually disappeared under acidification (Figure 6 c–e). The low concentration and coexistence of differently protonated species gives rise to the complex peak shape and causes difficulties in identification. However, the trends mentioned above do help us to understand the strict pH requirements of the synthesis.

Thus, in the SWNTs synthetic system, H^+ plays a significant role in mediating the surface charge of multiple Mo species, as well as their assembly properties. In addition, control experiments using low concentrations of a Mo source yield nothing, showing that the enrichment of Mo species, their assembly, and transformation into tubular structures is intimately related to the chemical potential. The results from experiments with Na_2MoO_4 as the raw material should also be understood as a result of the high concentration of Na^+ and Cl^-, which changes the interaction between charged Mo clusters and destroys their assembly.

On the other hand, it should be noted that ions always get enriched near the oil–water interface and in most cases it is the OH^- that accumulates around the microdroplet of oil in water. In this case, the hydrothermal environment disperses the thiol in water as droplets, which then attract specific aqueous species around them and facilitate the assembly at the interface. Nevertheless, the special role played by thiol and its reaction product disulfide is unique, since other oil–water interfaces did not result in the formation of SWNTs.

It is common knowledge that layered-structure nanotubes usually form through rolling up of the layers. In the case of MoO_3, the layer is a combination of many MoO_6 octahedrons. A tubular structure forms when the layer is bent in one direction, for example, the [001] direction, whereas 3D fullerene comes into being when the warping is complete. Direct evidence for this assumption was collected from products in which the tubular morphology had not been fully developed (Figure 7), since in many TEM images the nanotubes are found to coexist with some amorphous film, which should be their parent matrix (Figure 7a). Many of the nanotubes shown have one end formed with the other end fused with the film. Thus, it can be inferred that MoO_3 films are first formed at the oil–water interface through the assembly of Mo species with the assistance of thiol molecules. As the reaction proceeds, small pieces of a single layer roll into a tubular structure and are exfoliated from the whole film. This mechanism can be briefly illustrated as shown in Figure 1b.

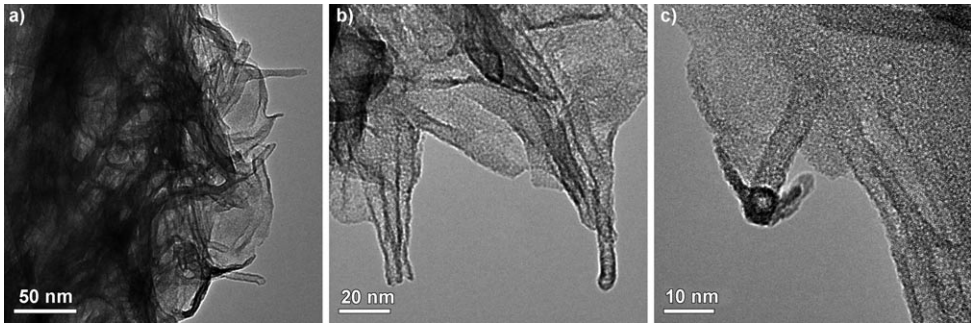

Figure 7. TEM images showing the transition state in the process of NT formation.

As for Mo-containing binary or ternary oxide compounds, MoO_6 octahedra are ubiquitous as structure-building units. A variety of Mo clusters in solution, from those containing several to those with hundreds of Mo centers, constitute another store of Mo and many of these clusters possess great similarity with those in molybdenum oxide bulk solid. For example, the polyoxometalate ion Mo_{248} contains two fragments of the type $Mo_{36}O_{96}(H_2O)_{24}$, the structure of which could be found in solid state Mo_5O_{14}.[23a] On the other hand, the complex polyoxometalate ion is believed to be assembled from simple ions through reduction, charge elimination, as well as combination, and this process is still considered as pivotal in polyoxometalate research. Hence, large polyoxometalate ions and bulk material, which might be considered as two forms of the same thing, can both be constituted from these simple ions, yet it is still a gray area that entities with dimensions between two and dozens of nm can be formed in the same way, which seems to be the most fasci-

nating range of nanoscience. Herein, we have investigated the transformation of small clusters into specific nanostructures with sizes of less than ten nanometers (Figure 8). Simi-

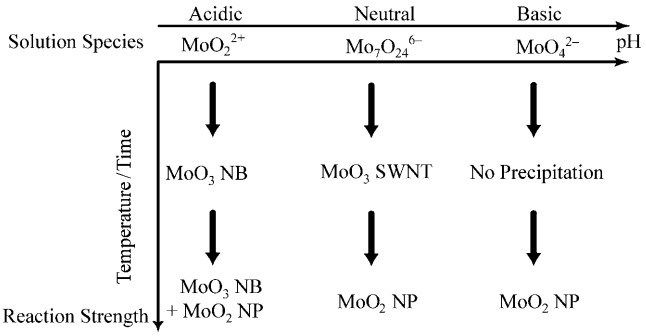

Figure 8. Correlation map of aqueous species, pH value, and reaction strength.

lar to the formation of various polyoxometalate macromolecules, the generation of MoO_3 nanostructures as SWNTs and inorganic fullerene is mediated by the pH value. The difference is that this process happens in a more intense hydrothermal environment, rather than the slow, mild reaction conditions for polyoxometalate formation, and it is sensitive to both the temperature and reaction time.

Finally, as a general principle in polyoxometalate chemistry, partially reduced Mo/O polyhedra always act as pivotal linkers of $Mo^{VI}O_6$ octahedra in the formation of large macromolecules; the generation of MoO_3 SWNTs and fullerenes may benefit from the partial reduction of Mo^{VI} by DT as these low oxidation Mo centers could provide the necessary curvature nodes and release the high stress induced in the rolling-up process of the rigid bilayer. The existence of low-oxidation-state Mo in the tube is also partially supported by the X-ray photoelectron spectroscopy of the SWNTs[26] and the color change of the aqueous solution (from colorless to blue) during the reaction.

Spectrum and electron sensitivity: The FTIR spectrum and confocal Raman spectrum were obtained from air-dried product (Figure 9). In the IR spectrum, the signal at 968 cm^{-1} is characteristic for the stretching mode of a Mo=O bond and that at 887 cm^{-1} is the result of the stretching mode of Mo with doubly connected O and the multiband between 700 and 400 cm^{-1} is from the complex bending mode of the Mo–O–Mo skeleton. The signal at 1400 cm^{-1} indicates significant hydroxylation of the SWNTs, whereas the broad absorption background above 1000 cm^{-1} is a result of water absorbed in the free form.[27] In the Raman spectrum, four characteristic bands at 947.1, 887.5, and 676.8/443.0 cm^{-1} correspond to the stretching modes of the terminal oxygen, the triply connected bridge oxygen, and the doubly connected bridge oxygen, respectively, showing a big shift from the values of bulky crystalline MoO_3 samples and other nanostructured MoO_3 compounds, although simi-

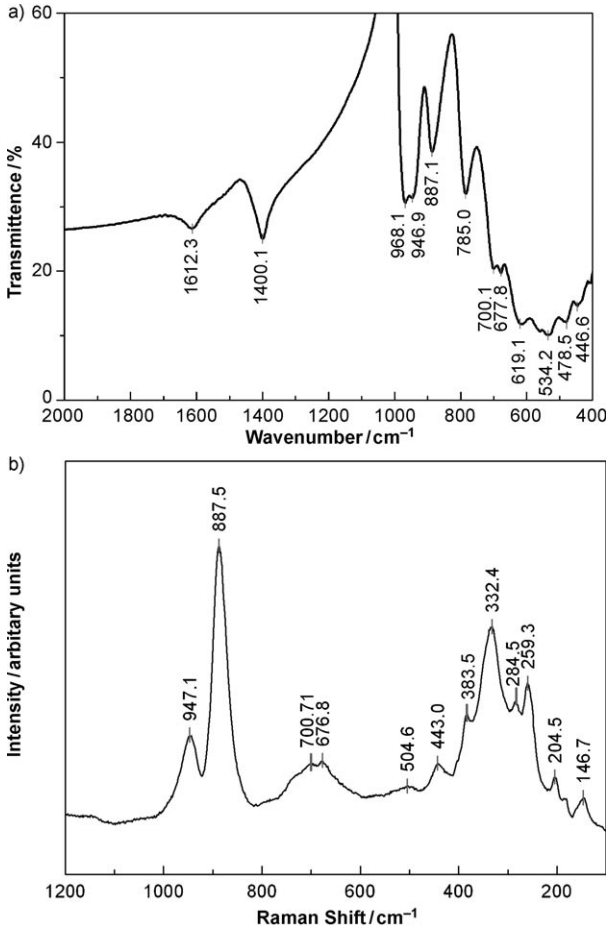

Figure 9. FTIR and Raman spectrum of MoO_3 SWNTs.

lar to those of amorphous MoO_3 films.[27,28] This can be explained by the highly strained nature of the 1D curved tubular double-layer structure, which should be different from that of the crystalline one.

MoO_3 has been reported to be electron sensitive and to respond to electron beam radiation and undergo a reduction and phase transformation.[29] This electron sensitivity is first illustrated by the observation of electron-beam-induced damage and crystallization of the NTs in TEM (Figure 10). With a high electron current illuminated over a single nanotube, it gradually split from one defect point and shrunk into two parts, which under further illumination, developed lattice fringes (as circled in Figure 10e and f), indicating a clear amorphous to crystalline transformation into MoO_2.

Electron sensitivity is further demonstrated by electron energy loss spectroscopy (EELS) characterization. Signals collected from an interweaved web of SWNTs after 5 and 25 min of continuous electron illumination show clear differences in the energy-loss near-edge structure (ELNES) of the O_K edge (shown here as peaks between 530 and 550 eV). As peaks A and B (Figure 11) represent the transition of O 1s electrons to the t_{2g} and e_g orbitals of Mo, respectively, and their strength is related to the number of unoccupied orbi-

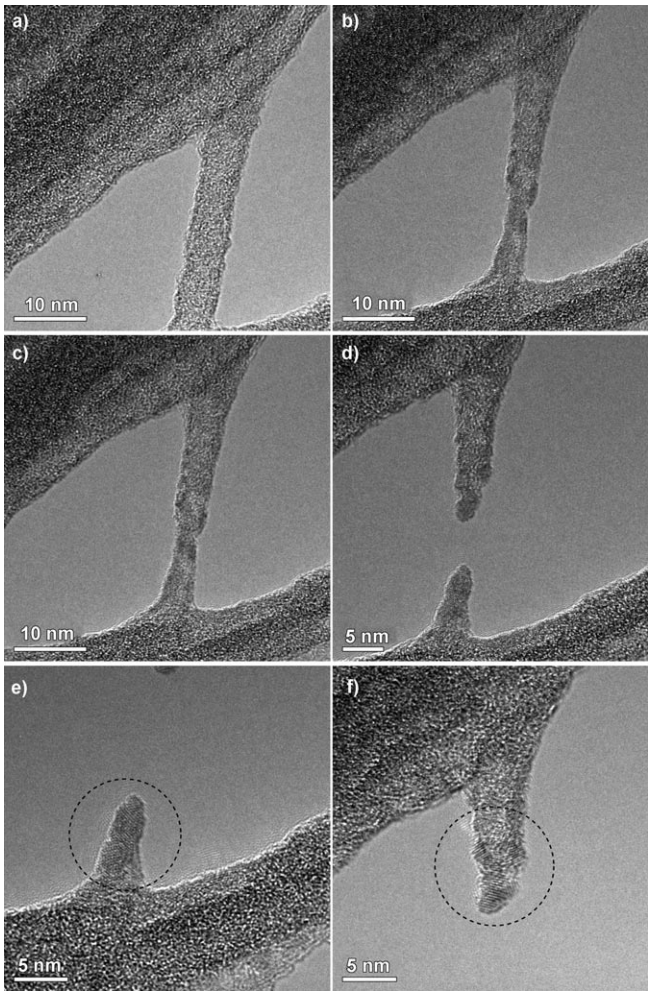

Figure 10. Consecutive TEM snapshots of the breaking and recrystallization process of SWNTs under illumination.

tals,[29] the variation in peak features shows a Mo^{VI} to Mo^{IV} transition of the sample under electron illumination.

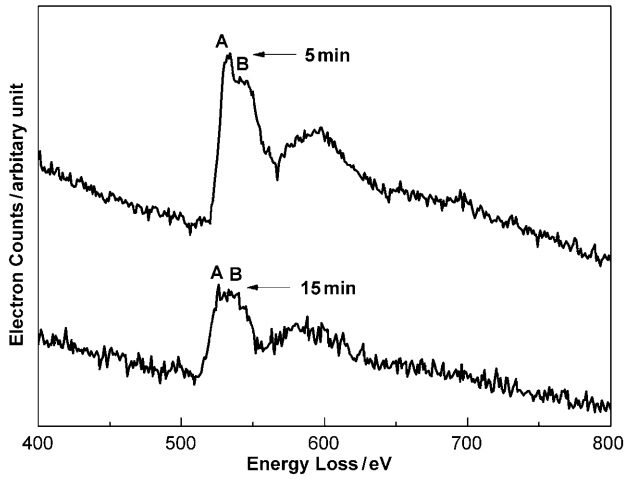

Figure 11. Time evolution of the EELS spectrum of SWNTs.

Conclusion

We have carried out a detailed investigation of the synthetic conditions for the formation of MoO_3 SWNTs in thiol–water biphasic systems. A cluster-based assembly and interface reaction mechanism is suggested by combining the viewpoints of nanostructure scientists and polyoxometalate chemists. TEM and other characterization methods provided support for our hypothesis. Finally, electron and photon sensitivity has also been studied through TEM to demonstrate the interesting properties of the SWNTs.

Experimental Section

Synthesis: For the synthesis of MoO_3 SWNTs, MA (H_2MoO_4, Beijing Chemical Reagent Plant, 0.5 g,) was mixed with distilled water and DT ($C_{12}H_{25}SH$, Sinopharm Chemical Reagent) and sealed in an autoclave. Then the reaction was heated to and kept at 190 °C for 32 h in an oven. After the autoclave was allowed to cool naturally, the upper organic phase was discarded and the turbid water phase was centrifuged at 10000 rpm for approximately 30 min. The black gluey precipitate at the bottom of the centrifuge tube was collected, washed several times with ethanol under ultrasonication conditions to remove most of the organic residues, and centrifuged to collect the solid. The product was stored in ethanol for further characterization. Alternatively, AM ($(NH_4)_6Mo_7O_{24}$) was used in place of MA with the addition of HCl (approximately 0.5 mmol), or octanethiol was used instead of dodecanethiol for the synthesis.

Characterization: For TEM observation, the product was dispersed in ethanol with ultrasonication and the dispersion was dropped upon a copper grid and examined, after drying, by a JEOL 2010 transmission electron microscope operated at 100 kV, whereas the HRTEM images were obtained from an FEI Tecnai G2 F20 S-Twin high-resolution transmission electron microscope under an acceleration voltage of 200 kV. The SEM images were obtained from a JEOL JSM-6700F scanning electron microscope. The crystal structures of the resulting material were determined by XRD on a Rigaku MiniFlex X-ray diffractometer by using $Cu_{K\alpha}$ radiation ($\lambda = 0.154$ nm) with 40 kV and 200 mA. Raman spectra were obtained from an RM2000 microscopic confocal Raman spectrometer (Renishaw PLC, England) equipped with a 633 nm laser beam. FTIR spectroscopy was performed on a Nicolet 560 spectrograph.

Acknowledgements

This work was supported by the NSFC (grant nos. 20725102, 20921001), the Foundation for the Author of National Excellent Doctoral Dissertation of P. R. China, the Fok Ying Tung Education Foundation (grant no. 111012), and the State Key Project of Fundamental Research for Nanoscience and Nanotechnology (grant no. 2006CB932301).

[1] S. Iijima, *Nature* **1991**, *354*, 56–58.
[2] a) W. Lu, C. M. Lieber, *Nat. Mater.* **2007**, *6*, 841–850; b) R. H. Baughman, A. A. Zakhidov, W. A. D. Heer, *Science* **2002**, *297*, 787–792.
[3] a) C. R. Martin, P. Kohli, *Nat. Rev. Drug Discovery* **2003**, *2*, 29–37; b) A. Bianco, K. Kostarelos, M. Prato, *Curr. Opin. Chem. Biol.* **2005**, *9*, 674–679.
[4] a) X. Pan, Z. Fan, W. Chen, Y. Ding, H. Luo, X. Bao, *Nat. Mater.* **2007**, *6*, 507–511; b) G. K. Mor, K. Shankar, M. Paulose, O. K. Varghese, C. A. Grimes, *Nano Lett.* **2005**, *5*, 191–195.

[5] J. Kong, N. R. Franklin, C. W. Zhou, M. G. Chapline, S. Peng, K. J. Cho, H. J. Dai, *Science* **2000**, *287*, 622–625.
[6] W. A. De Heer, A. Chatelain, D. Ugarte, *Science* **1995**, *270*, 1179–1180.
[7] A. Srivastava, O. N. Srivastava, S. Talapatra, R. Vajtai, P. M. Ajayan, *Nat. Mater.* **2004**, *3*, 610–614.
[8] D. Wang, H. Fang, F. Li, Z. Chen, Q. Zhong, G. Q. Lu, H. Cheng, *Adv. Funct. Mater.* **2008**, *18*, 3787–3793.
[9] J. Goldberger, R. Fan, P. D. Yang, *Acc. Chem. Res.* **2006**, *39*, 239–248.
[10] a) R. Tenne, *Nature* **1992**, *360*, 444–446; b) M. Hershfinkel, L. A. Gheber, V. Volterra, J. L. Hutchison, L. Margulis, R. Tenne, *J. Am. Chem. Soc.* **1994**, *116*, 1914–1917.
[11] F. Krumeich, H.-J. Muhr, M. Niederberger, F. Bieri, B. Schnyder, R. Nesper, *J. Am. Chem. Soc.* **1999**, *121*, 8324–8331.
[12] Y. R. Hacohen, E. Grunbaum, R. Tenne, J. Sloan, J. L. Hutchison, *Nature* **1998**, *395*, 336–337.
[13] Y. D. Li, J. W. Wang, Z. X. Deng, Y. Y. Wu, X. M. Sun, D. P. Yu, P. D. Yang, *J. Am. Chem. Soc.* **2001**, *123*, 9904–9905.
[14] a) M. Remskar, A. Mrzel, Z. Skraba, A. Jesih, M. Ceh, J. Demsÿar, P. Stadelmann, F. Levy, D. Mihailovic, *Science* **2001**, *292*, 479–481; b) S. Mukherjee, V. M. Bartlow, S. Nair, *Chem. Mater.* **2005**, *17*, 4900–4909; c) C. D. Malliakas, M. G. Kanatzidis, *J. Am. Chem. Soc.* **2006**, *128*, 6538–6539; d) H. Yang, C. Wang, Z. Su, *Chem. Mater.* **2008**, *20*, 4484–4488.
[15] C. Bechinger, S. Ferrere, A. Zaban, J. Sprague, B. A. Gregg, *Nature* **1996**, *383*, 608–610.
[16] M. Ferroni, V. Guidi, G. Martinelli, M. Sacerdoti, P. Nelli, G. Sberveglieri, *Sens. Actuators B* **1998**, *48*, 285–288.
[17] J. N. Yao, K. Hashimoto, A. Fujishima, *Nature* **1992**, *355*, 624–626.
[18] L. Mai, B. Hu, W. Chen, Y. Qi, C. Lao, R. Yang, Y. Dai, Z. L. Wang, *Adv. Mater.* **2007**, *19*, 3712–3716.
[19] J. Zhou, S. Z. Deng, N. S. Xu, J. Chen, J. C. She, *Appl. Phys. Lett.* **2003**, *83*, 2653–2655.
[20] L. Fang, Y. Shu, A. Wang, T. Zhang, *J. Phys. Chem. C* **2007**, *111*, 2401–2408.
[21] X. L. Li, J. F. Liu, Y. D. Li, *Appl. Phys. Lett.* **2002**, *81*, 4832–4834.
[22] T. Liu, Y. Xie, B. Chu, *Langmuir* **2000**, *16*, 9015–9022.
[23] a) A. Müller, P. Kögerler, C. Kuhlmann, *Chem. Commun.* **1999**, 1347–1358; b) A. Müller, C. Serain, *Acc. Chem. Res.* **2000**, *33*, 2–10; c) A. Müller, F. Peters, M. T. Pope, D. Gatteschi, *Chem. Rev.* **1998**, *98*, 239–271.
[24] X. Wang, Q. Peng, Y. Li, *Acc. Chem. Res.* **2007**, *40*, 293–303.
[25] a) Z. Zhuang, Q. Peng, X. Wang, Y. Li, *Angew. Chem.* **2007**, *119*, 8322–8325; *Angew. Chem. Int. Ed.* **2007**, *46*, 8174–8177; b) Z. Zhuang, Q. Peng, B. Zhang, Y. Li, *J. Am. Chem. Soc.* **2008**, *130*, 10482–10483.
[26] S. Hu, X. Wang, *J. Am. Chem. Soc.* **2008**, *130*, 8126–8127.
[27] L. Seguin, M. Figlarz, R. Cavagnat, J. C. Lassegues, *Spectrochim. Acta Part A* **1995**, *51*, 1323–1344.
[28] K. Ajito, L. A. Nagahara, D. A. Tryk, K. Hashimoto, A. Fujishima, *J. Phys. Chem.* **1995**, *99*, 16383–16388.
[29] D. Wang, D. S. Su, R. Schlögl, *Z. Anorg. Allg. Chem.* **2004**, *630*, 1007–1014.

Received: July 29, 2009
Published online: December 28, 2009

